

Electron-impact vibrational excitation of isocyanic acid HNCO

Ragesh Kumar T. P. ¹, P. Nag ¹, M. Ranković ¹, R. Čurík,^{1,*} A. Knížek ¹, S. Civiš ¹, M. Ferus,¹ J. Trnka ²,
K. Houfek ², M. Čížek ^{2,†} and J. Fedor ^{1,‡}

¹*J. Heyrovský Institute of Physical Chemistry, Czech Academy of Sciences, Dolejškova 3, 18223 Prague, Czech Republic*

²*Institute of Theoretical Physics, Faculty of Mathematics and Physics, Charles University, Holešovičkách 2, 180 00 Prague, Czech Republic*



(Received 29 October 2020; accepted 8 December 2020; published 24 December 2020)

In a combined experimental and theoretical study, we probe the vibrational excitation of isocyanic acid induced by electron impact in the energy range up to 5 eV. Experimentally, we report differential elastic and vibrationally inelastic cross sections at the scattering angle of 135°. Theoretically, we characterize the involved resonant states using a regularized analytical continuation method. We also apply a nonlocal resonance model to calculate cross sections for vibrational mode that involves the N-H stretching motion. The model reproduces all the features observed in the experiment: efficient excitation at threshold, sharp cusps in the excitation functions, and the formation of an A' shape resonance. There is a second (A'') resonance visible in the spectra; however, it excites only selected vibrational modes. The origins of this selectivity are discussed.

DOI: [10.1103/PhysRevA.102.062822](https://doi.org/10.1103/PhysRevA.102.062822)

I. INTRODUCTION

HNCO is the simplest molecule containing all four basic chemical elements that are constituents of a broad range of organic molecules and biomolecules. As such, it has been attracting attention as a possible important precursor in prebiotic chemistry [1,2]. This interest is intensified by the fact that it is an abundant interstellar molecule: It was among the very early molecules to be detected in space, in the Galactic center clouds [3]. It is also abundant in dark clouds, such as TMC-1 [4], and translucent clouds [5]. In a survey of 81 molecular clouds, its detection rate was 70% [6]. It was also detected in hot cores [7], high-mass young stellar objects [8], molecular outflows [9], and comets [10].

It is believed that in the interstellar space with low particle density, the decomposition reactions are to a large degree initiated by ultraviolet light, x rays, and cosmic rays (most of which are high-energy protons). When such high-energy radiation interacts with interstellar icy grains that probably serve as reservoirs for chemical reactions, it produces an avalanche of secondary electrons. One high-energy proton may release 10^4 secondary electrons in its passage through a single ice-covered dust grain [11]. These secondary electrons have mean kinetic energies in the region of units and tens of electronvolts [11]. In this paper, we address the question of how such low-energy electrons excite HNCO vibrationally. Previous works on other astrophysically relevant unsaturated molecules such as C_4H_2 [12], HC_3N [13], and $NCCN$ [14] have shown that electrons can be very efficient in mediating the vibrational excitation, although various normal modes can be excited selectively.

HNCO is an interesting target for electron scattering experiments also from a purely fundamental point of view. First, due to the two double bonds, the molecule has low-lying unoccupied π^* orbitals. These are expected to give rise to π^* shape resonances. Due to the nonlinear structure of the molecule (CNH angle is 124°), the lower of these resonances (A' symmetry) has a mixed π^*/σ^* character from the point of view of the N-H bond. Second, HNCO is a polar molecule with the dipole moment of 1.6 Debye [15]. We have recently shown [16] that the combination of these properties leads to the dissociative electron attachment (DEA) cross section which is rich in fine features. There, we presented a one-dimensional nonlocal resonance model which reproduced the experimental DEA cross section very well. With a simplified description, such electron-induced dissociation can be viewed as a multistep process: The electron is attached, change in the electronic configuration induces motion of the nuclei, and the bond is cleaved, producing stable anionic fragment and a neutral radical (in this case, $NCO^- + H$). If, however, the electron detaches during this process, the configuration of nuclei is different than the neutral ground-state minimum and as a result, the molecule is left vibrationally excited. Probing the vibrational excitation channels thus provides information about earlier stage of the nuclear motion than the DEA. It thus represents an independent test of the theoretical model. Additionally, the ability to follow the different normal modes brings the information about the direction of the induced motion upon the resonance formation.

II. EXPERIMENTAL SETUP

The electron scattering experiments were performed on the electrostatic spectrometer with the hemispherical electron monochromator and analyzer [17,18]. Electrons scattered on the effusive beam of pure sample gas were analyzed at a fixed scattering angle. The energy of the incident beam was

*roman.curik@jh-inst.cas.cz

†cizek@mbox.troja.mff.cuni.cz

‡juraj.fedor@jh-inst.cas.cz

calibrated on the 19.365-eV 2^2S resonance in helium. Combined electron-energy resolution was 17 meV. The absolute elastic scattering cross section was calibrated against the one of helium using a relative flow method.

The present data were taken by operating the spectrometer in two different measurement modes. In the first one, the electron energy-loss spectrum of HNCO was measured at a constant incident energy. Here the electron monochromator was set to pass the electrons with the fixed incident energy and the analyzer was scanned for residual energy of scattered electrons. The signal is typically plotted as a function of the difference between the incident and residual energy, which is the energy loss of the electron. In the second mode of the measurement, the excitation functions of the given energy losses were recorded. Here, both monochromator and analyzer were scanned for the entire range of electron energies, with their difference kept constant.

All the present data were taken at a fixed scattering angle of 135° . This is the highest angle which is mechanically achievable due to constraints given by the physical space occupied by the monochromator and analyzer. The preference for high scattering angle in this work was driven by the interest in the resonant processes. It is well established that the cross section for direct dipole scattering is forward peaked [19,20], and the resonant processes are thus best visible at high scattering angles.

The HNCO sample was synthesized by a pyrolysis of cyanouric acid [21]. During the measurements, the sample was kept at the temperature of solid CO_2 (-78.5°C), only slightly above the HNCO melting temperature of (-86°C). The low temperature contributes to the purity of sample vapor since it keeps partial pressures of possible volatile impurities low.

III. THEORY

A. RAC analysis of the shape resonances

The shape resonances were analyzed by using the regularized analytic continuation (RAC) method [22,23]. In this method, an additional perturbation field V is applied to the molecular Hamiltonian H , $H \rightarrow H + \lambda V$. The attractive one-electron operator λV makes the quasibound resonant state truly bound, and therefore it can be described by the standard quantum chemistry software. Several forms of the perturbation potential (e.g., Coulomb, Gaussian, and their product [24–26]) do not require any software modifications of the quantum chemistry programs. In the present study, the nuclear potential of the molecule was utilized as the perturbation field, i.e.,

$$V = \sum_{A=1}^4 \sum_i \frac{Z_A}{|\vec{r}_i - \vec{R}_A|}, \quad (1)$$

where \vec{r}_i are the electronic coordinates, vectors \vec{R}_A denote positions of the H, N, C, and O atoms, and Z_A are their corresponding nuclear charges. The chosen form of the perturbation potential has provided reasonably accurate A' resonance parameters in our previous DEA study on this molecular system [16]. The electron affinities $\Delta E(\lambda) = \kappa^2(\lambda)$ in the presence of the perturbation potential were computed

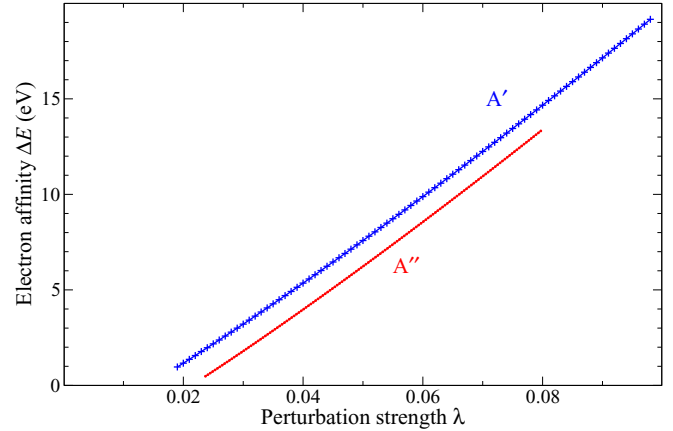


FIG. 1. Computed vertical electron affinities $\Delta E(\lambda)$ for the two π^* resonances at the equilibrium geometry. The data points for the in-plane A' resonance are shown as crosses, while the data points for the out-of-plane resonance A'' are displayed by small circles (overlapping into a line).

by the coupled clusters (CCSD-T) method [27,28] as implemented in MOLPRO 2010 package of quantum chemistry programs [29] with the Dunning's augmented correlation-consistent basis set [30] (aug-cc-pVTZ).

The data points used in the present study are shown in Fig. 1 for the two π^* resonances examined. The RAC method continues the real-valued affinity momenta $\kappa(\lambda) = \sqrt{\Delta E(\lambda)}$ to the complex plane by applying the Padé approximation on the inverse function $\lambda(\kappa)$. We utilized the RAC [3/1] Padé approximation [23],

$$\lambda^{[3/1]}(\kappa) = \lambda_0 \frac{(\kappa^2 + 2\alpha^2\kappa + \alpha^4 + \beta^2)(1 + \delta^2\kappa)}{\alpha^4 + \beta^2 + \kappa[2\alpha^2 + \delta^2(\alpha^4 + \beta^2)]}, \quad (2)$$

where λ_0 , α , β , δ are the fitting parameters that provide the resonance energy $E_r = \beta^2 - \alpha^4$ and the resonance width $\Gamma = 4\alpha^2|\beta|$.

At the equilibrium geometry of the neutral HNCO, the A' and A'' resonances were calculated at 2.49 eV ($\Gamma = 0.48$ eV) and 4.10 eV ($\Gamma = 0.80$ eV), respectively.

B. Nonlocal model for the N-H stretch vibration

For energies above 1.16 eV, the electron scattering process competes with dissociative electron attachment in which NCO^- anion is created. In our previous work, we have developed a nonlocal resonance model to treat this process [16]. The same model can be used to describe the vibrational excitation of NH stretch mode by the electron impact. The ability of this model to describe the current vibrational excitation data is an independent check of the model and the underlying assumptions and validates also our understanding of the dissociative electron attachment process.

The nonlocal resonance model for the excitation of HNCO along NH-stretch coordinate and its construction is described in detail in Ref. [16]. Here we summarize briefly the key information and show the potential energy curves in Fig. 2. The model is based on the Fano model of discrete-state interaction with continuum that can be used to parametrize the interaction of incoming electron with the molecule [31]

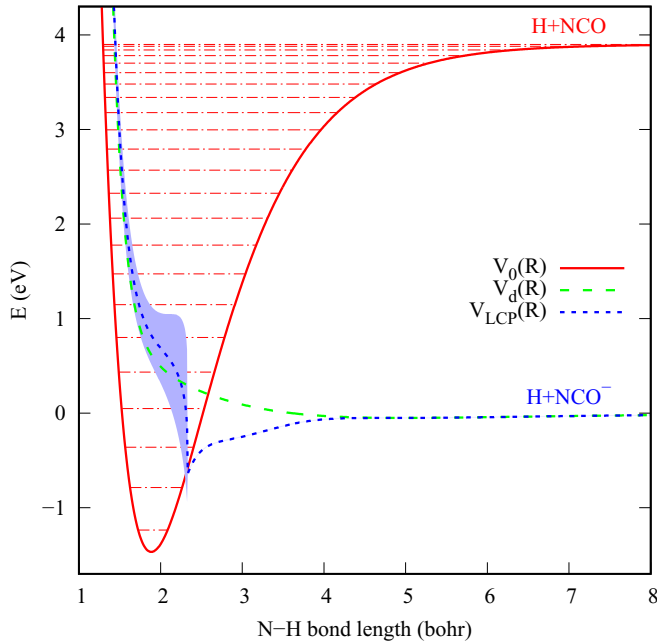


FIG. 2. Potential energy curves $V_0(R)$, $V_d(R)$, and $V_{LCP}(R)$ for the model describing N–H stretch dynamics. Vibrational energies are included with dash-dotted lines and the width of the fixed-nuclei resonance (\pm imaginary part of V_{LCP}) is marked by extent of the blue-shaded area.

for each fixed position of nuclei. In our case, the discrete state describes the narrow resonance at the equilibrium geometry of HNCO which changes its character with stretching NH distance until it becomes a bound electronic state corresponding to the NCO^- ion and the H atom for large NH separations. The model is fully described by potential energy curves (cuts of the full surfaces along the NH bond) of the neutral molecule and the anion discrete state and also by the discrete-state-continuum coupling, which is closely related to the width of the anion resonance. The potential energy curves for electronically bound states were calculated in Ref. [16] using the coupled-clusters approach, CCSD-T/aug-cc-pVTZ [27,28,30], and the resonance parameters were extracted using regularized analytic continuation (RAC) method [22,32]. To fully characterize the electron-molecule interaction in the model and to fix the discrete-state-continuum coupling, we performed the fixed-nuclei R -matrix scattering calculations. The resulting cross sections for the A' symmetry are shown in Fig. 3 for several N–H distances around the equilibrium geometry, showing resonances in the range 1.5–3.5 eV corresponding to the 2.5-eV resonance in the experimental cross sections. To justify the one-dimensional approach, we also verified that the energy of the discrete state depends only weakly on the CNH-bending angle. We thus finally constructed in Ref. [16] the nonlocal resonance model that is fully based on *ab initio* calculations. The only additional tuning in the model was the shift of the dissociative attachment threshold caused by relaxation of the geometry of the NCO^- fragment. This relaxation cannot be described by a one-dimensional model. Here we use this final model to calculate the vibrational excitation cross sections of the

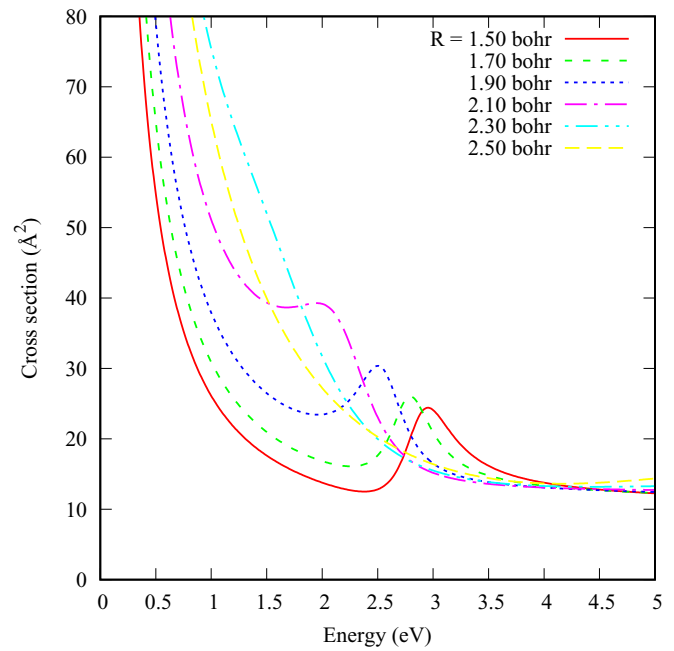


FIG. 3. Fixed-nuclei scattering cross sections for the A' symmetry determined from the R -matrix data used in Ref. [16] to construct the model for the N–H stretch dynamic for several NH-bond lengths R . Equilibrium bond length is approximately $R = 1.9$ bohr.

NH-stretch mode. Numerical treatment follows the procedure developed for the nonlocal resonance theory in our earlier works [33–35]. To check the sensitivity of the resulting vibrational excitation cross sections on the fitting procedure in the construction of the nonlocal model, we constructed two additional models with slightly changed assumptions on the analytic form of the model functions. We found that the results are quite robust with respect to these changes, with overall shape of the excitation curves unchanged and the absolute magnitude of the cross sections remaining within 30% of the original data.

IV. RESULTS AND DISCUSSION

Figure 4 shows the electron energy-loss spectrum of HNCO recorded at the constant incident energy of 2.2 eV and at the scattering angle of 135° . The peak at 0 eV (no energy loss) corresponds to the elastic scattering and the higher lying peaks to the excitation of individual vibrational modes. The assignment of the peaks has been done based on the optical infrared (IR) spectra of HNCO [36]; the mode numbering follows Ref. [36]. HNCO has six normal modes. All of them are excited by the electron impact. Apart from these, there are weak peaks visible in the spectra which are overtones and/or combination bands. Of these, the strongest is the first overtone of the NH stretch mode. The low-lying closely spaced bending modes ν_4 to ν_6 are not fully resolved by the spectrometer.

Figures 5 and 6 show the excitation curves of the individual vibrations. They are divided into these two figures depending on whether the one-dimensional nonlocal resonance model provides the theoretical prediction of the corresponding cross

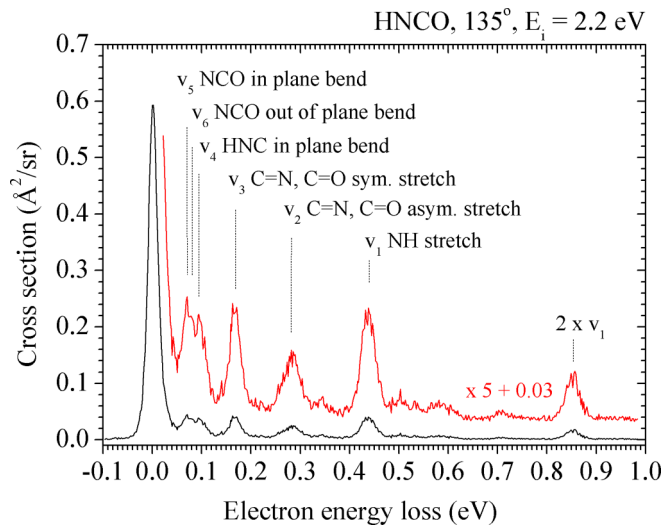


FIG. 4. Electron energy-loss spectrum of HNCO recorded at the constant incident energy of 2.2 eV and at the scattering angle of 135° .

sections. We first discuss Fig. 5, i.e., the elastic scattering and the N-H stretch containing vibrations.

There is a very good qualitative correspondence between the experimental and calculated data. The excitation curves for all three channels show a threshold peak of varying intensity. This is typical for dipolar systems [37,38]: The slow incoming electron interacts with the molecule via the long-range potential, which leads to bond deformation, and as it departs, the molecule is left vibrationally excited. The threshold peak for the NH stretch overtone ($0 \rightarrow 2$) transition is very weak. This is expected—the cross section for vibrational excitation in the Born approximation is proportional to IR intensity of the given transition [38]. This is, in the harmonic approximation, zero for the first overtone. In the current model, the threshold peak in the $0 \rightarrow 1$ curve is much weaker than in experiment, but this may well be consequence of reduced dimensionality of the model. The second dominant feature in the cross sections is the broad resonance centered between 2 and 3 eV. This is the ${}^2A'$ resonance, predicted by the RAC method at 2.49 eV. In the experimental elastic cross section, it is barely visible, but in the $0 \rightarrow 1$ and $0 \rightarrow 2$ NH stretch transitions, it is very clear. The $0 \rightarrow 2$ excitation curve seems to have the maximum shifted to lower energies; actually it rather looks as a small “side” maximum at the left flank of the broad peak. However, this is most likely the effect of a nitrogen impurity in the sample. The frequency of the $N_2(0 \rightarrow 3)$ transition (876 meV) accidentally overlaps with the $NH(0 \rightarrow 2)$ transition. The excitation function of $N_2(0 \rightarrow 3)$ is known to have very strong oscillatory structure with the maximum at 2.2 eV. Even the trace amount of the residual nitrogen can be responsible for the observed difference in the shape of the $NH(0 \rightarrow 1)$ and $NH(0 \rightarrow 2)$ resonance bands.

Additionally, the excitation cross sections show a number of sharp features. These are similar to those observed in low-energy electron scattering from hydrogen halides. From the theoretical point of view, this is not surprising, since the shape of the current model functions is qualitatively similar

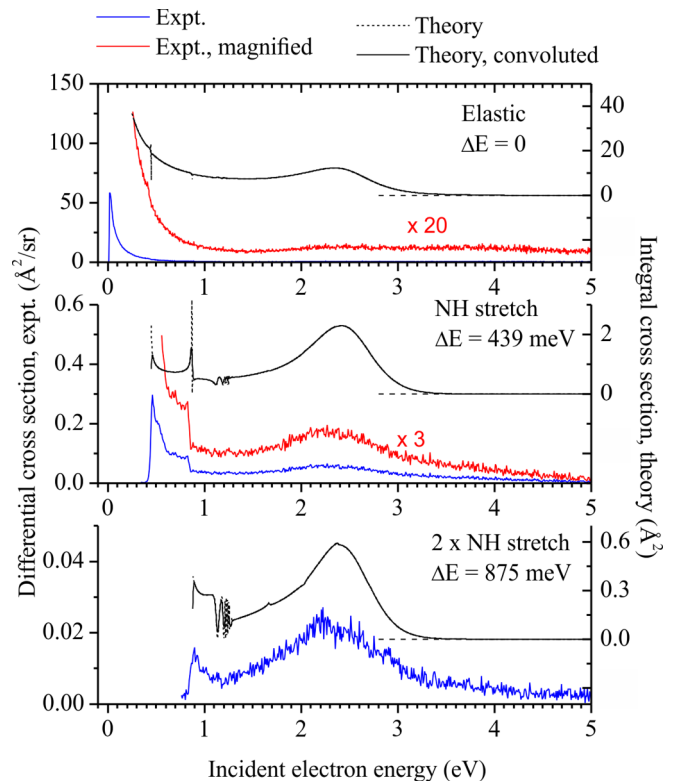


FIG. 5. Excitation curves for elastic scattering ($0 \rightarrow 0$), the NH stretch vibration ($0 \rightarrow 1$), and its first overtone ($0 \rightarrow 2$). The experimental data (noisy lines, left axis) are the differential cross sections at the 135° scattering angle, and the theoretical data (smooth lines, right axis) are the calculated integral cross section. For the sake of clarity, the experimental and theoretical curves are vertically offset. The full theoretical line is the calculated cross section convoluted with a Gaussian of 17-meV FWHM.

to those used for treatment of hydrogen halides [39,40]. The different channels are strongly coupled, which results in the presence of the Wigner cusps at opening of higher channels. These cusps in the elastic and $0 \rightarrow 1$ cross sections below 1.1 eV are combined with peaks and dips due to vibrational Feshbach resonances known from scattering of electrons [41] and positrons [42] from molecules. The most prominent cusp is visible in the $0 \rightarrow 1$ cross section at the $0 \rightarrow 2$ threshold energy 0.86 eV; its shape agrees very well in theory and experiment. Theory also predicts a very narrow cusp in the elastic cross section at the $0 \rightarrow 1$ threshold energy 0.44 eV, which is smoother when convoluted according to experimental resolution. Still, there is a hint of a structure in the experimental elastic cross section at this energy. The predicted cusps in the $0 \rightarrow 2$ cross sections above 1.3 eV are unfortunately too weak to be resolved in the experiment. The same is true about the boomerang oscillations [43] visible in the theoretical data below the dissociative attachment threshold at 1.1–1.2 eV. This is a pity because we also do not know if extension of the theoretical model by accounting for other vibrational modes will not suppress these structures. This problem will be subject of future theoretical study.

Figure 6 shows the excitation curves for other HNCO normal modes. It should be remembered that the bending modes

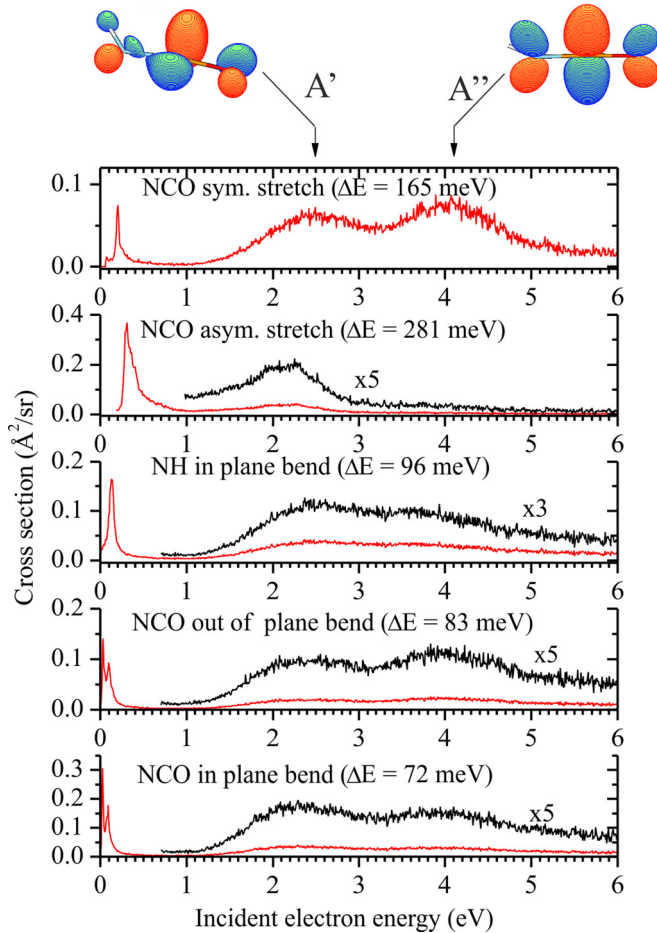


FIG. 6. Excitation curves for the normal modes, which involve multidimensional motion, measured at the 135° scattering angle. The two arrows on top mark the RAC-calculated positions of the A' and A'' shape resonances. The isosurfaces are the singly occupied HNCO^- orbitals in the reference determinant used in the CCSD-T calculations.

are not fully resolved and the individual excitation functions contain contributions of the neighboring mode. This is manifested, for example, in the seemingly doubled threshold peaks in the lowest two panels of Fig. 6; it is an artifact explained in detail in Ref. [44]. Anyhow, apart from the threshold peaks (their intensities again reflect the IR activities of the modes), the spectra are dominated by two resonances. These are the A' resonance, already discussed above, and the A'' resonance. Experimentally, the A'' band is centered around 4 eV, which is in an excellent agreement with the RAC calculated value of 4.10 eV.

The individual modes are excited selectively by the formation of resonances, and especially the A'' is visible only in the NCO symmetric stretch and in the bending modes. As seen from the orbital isosurface in Fig. 6, this is an out-of-plane π^* resonance. The first type of modes which it is expected to excite are thus those that break the planar symmetry. Indeed, it is strong in the NCO out-of-plane bend. In the two in-plane bends, it is visible as much weaker and this is probably again an effect of instrumental resolution. Additionally, the reso-

nance will be visible in modes involving a stretching along the N–C and C–O bonds that are weakened by the presence of the resonant electron. Hence, it is strong in the NCO symmetric stretch mode and invisible in the HN stretch mode in Fig. 5.

In light of this, the absence of the A'' resonance in the NCO asymmetric stretch excitation curve may be surprising. However, this phenomena can be explained by a high similarity between the present out-of-plane π^* resonance and the well-known Π_u shape resonance of CO_2 situated around 3.6 eV [45]. HNCO is isoelectronic with CO_2 and is only slightly bent with respect to the carbon atom. Frequency of the CO_2 symmetric stretch is only different by 7 meV than the one in HNCO and of the asymmetric stretch by 10 meV [46]. Furthermore, the top panel of Fig. 6 shows that the A'' resonance is quite symmetric with respect to interchange of the nitrogen and oxygen atoms. These observations set up conditions for the A'' resonant curve having even symmetry along the asymmetric stretch coordinate ν_2 , as occurs in the case of CO_2 [47]. The resulting vibrational excitation cross section is then strongly suppressed for the initial and final vibrational states of different symmetry along the asymmetric stretch coordinate, as was observed in CO_2 both experimentally [45] and theoretically [47]. From the same reason, the A'' resonance is not manifested in the $\nu_2(0 \rightarrow 1)$ asymmetric stretch transition of HNCO .

V. CONCLUSIONS

In conclusion, we probed the vibrational excitation of isocyanic acid by low-energy electron impact. Experimentally, we observe the excitation of all six normal modes. Their excitation curves are rich on various features: They exhibit threshold peaks of varying intensities and two resonances which excite the vibrations selectively. Additionally, the N–H stretch vibration shows a pronounced sharp cusp at the opening of the next vibrational level.

The RAC calculation predicts positions of the two shape resonances in an excellent agreement with the experiment. The properties of their wave functions provide reasoning behind the mode selectivity of the vibrational excitation. The nonlocal resonance model, which was originally constructed to describe the N–H bond cleavage via dissociative electron attachment [16], was used here to calculate the elastic scattering cross section and the cross sections for the $0 \rightarrow 1$ and $0 \rightarrow 2$ excitations of the N–H stretch mode. The model reproduces all the experimentally observed effects and additionally predicts finer features which are hidden in the experiment due to insufficient signal to noise ratio. We would like to stress that even though the model is one dimensional, the qualitative agreement with the present experiment confirms that it describes the N–H stretch motion very well. Still, the considerable excitation of all the other normal modes observed experimentally shows that the dynamics is inherently multidimensional. The addition of other vibrational modes into the nonlocal model would be desirable in the future in order to describe the low-energy electron interaction with HNCO fully.

ACKNOWLEDGMENTS

This work was supported by Projects No. 20-11460S (J.F.), No. 19-20524S (M.Č., K.H., and J.T.), No. 19-03314S

(M.F.), and No. 18-02098S (R.Č.) of the Czech Science Foundation. M.F. also acknowledges ERDF/ESF “Centre of

Advanced Applied Sciences” (No. CZ.02.1.01/0.0/0.0/16_019/0000778).

-
- [1] G. Fedoseev, S. Ioppolo, D. Zhao, T. Lamberts, and H. Linnartz, *MNRAS* **446**, 439 (2015).
- [2] L. Song and J. Kastner, *Phys. Chem. Chem. Phys.* **18**, 29278 (2016).
- [3] L. S. D. Buhl, *Astrophys. J.* **177**, 619 (1972).
- [4] R. L. Brown, *Astrophys. J.* **248**, L119 (1981).
- [5] B. E. Turner, R. Terzieva, and E. Herbst, *Astrophys. J.* **518**, 699 (1999).
- [6] I. Zinchenko, C. Henkel, and R. Q. Mao, *Astron. Astrophys.* **361**, 1079 (2000).
- [7] F. P. Helmich and E. F. van Dishoeck, *Astron. Astrophys. Suppl. Ser.* **124**, 205 (1997).
- [8] S. E. Bisschop, J. K. Jorgensen, E. F. van Dishoeck, and E. B. M. de Wachter, *Astron. Astrophys.* **465**, 913 (2007).
- [9] N. J. Rodriguez-Fernandez, M. Tafalla, F. Gueth, and R. Bachiller, *Astron. Astrophys.* **516**, A98 (2010).
- [10] D. C. Lis, J. Keene, K. Young, T. G. Phillips, D. Bockelée-Morvan, J. Crovisier, P. Schilke, P. F. Goldsmith, and E. A. Bergine, *Icarus* **130**, 355 (1997).
- [11] S. Pimblott and J. la Verne, *Radiat. Phys. Chem.* **76**, 1244 (2007).
- [12] M. Allan, O. May, J. Fedor, B. C. Ibănescu, and L. Andric, *Phys. Rev. A* **83**, 052701 (2011).
- [13] M. Ranković, P. Nag, M. Zawadzki, L. Ballauf, J. Žabka, M. Polášek, J. Kočišek, and J. Fedor, *Phys. Rev. A* **98**, 052708 (2018).
- [14] P. Nag, R. Čurík, M. Tarana, M. Polášek, M. Ehara, T. Sommerfeld, and J. Fedor, *Phys. Chem. Chem. Phys.* **22**, 23141 (2020).
- [15] J. N. Shoolery, R. G. Shulman, and D. M. Yost, *J. Chem. Phys.* **19**, 250 (1951).
- [16] M. Zawadzki, M. Čížek, K. Houfek, R. Čurík, M. Ferus, S. Civiš, J. Kočišek, and J. Fedor, *Phys. Rev. Lett.* **121**, 143402 (2018).
- [17] M. Allan, *J. Phys. B: Atom. Molec. Phys.* **25**, 1559 (1992).
- [18] M. Allan, *J. Phys. B: Atom. Molec. Phys.* **38**, 3655 (2005).
- [19] M. Allan, *J. Electr. Spectr. Rel. Phenomena* **48**, 219 (1989).
- [20] M. Allan, M. Lacko, P. Papp, Š. Matejčík, M. Zlatar, I. I. Fabrikant, J. Kočišek, and J. Fedor, *Phys. Chem. Chem. Phys.* **20**, 11692 (2018).
- [21] G. Fischer, J. Geith, T. M. Klapotke, and B. Krumm, *Z. Naturforsch.* **57**, 19 (2002).
- [22] J. Horáček, I. Paidarová, and R. Čurík, *J. Chem. Phys.* **143**, 184102 (2015).
- [23] R. Čurík, I. Paidarová, and J. Horáček, *Europ. Phys. J. D* **70**, 146 (2016).
- [24] A. F. White, M. Head-Gordon, and C. W. McCurdy, *J. Chem. Phys.* **146**, 044112 (2017).
- [25] T. Sommerfeld, J. B. Melugin, P. Hamal, and M. Ehara, *J. Chem. Theory Comput.* **13**, 2550 (2017).
- [26] R. Čurík, I. Paidarová, and J. Horáček, *Phys. Rev. A* **97**, 052704 (2018).
- [27] P. J. Knowles, C. Hampel, and H. Werner, *J. Chem. Phys.* **99**, 5219 (1993).
- [28] M. J. Deegan and P. J. Knowles, *Chem. Phys. Lett.* **227**, 321 (1994).
- [29] H. J. Werner, P. J. Knowles, R. Lindh, F. R. Knizia, F. R. Manby, M. Schütz *et al.*, MOLPRO, version 2010.1, a package of *ab initio* programs.
- [30] T. H. Dunning, *J. Chem. Phys.* **90**, 1007 (1989).
- [31] W. Domcke, *Phys. Rep.* **208**, 97 (1991).
- [32] J. Horáček, I. Paidarová, and R. Čurík, *J. Phys. Chem. A* **118**, 6536 (2014).
- [33] P. Čárský and R. Čurík (eds.), *Low-Energy Electron Scattering from Molecules, Biomolecules, and Surfaces* (CRC Press, Boca Raton, FL, 2012).
- [34] M. Čížek, J. Horáček, A.-C. Sergenton, D. B. Popović, M. Allan, W. Domcke, T. Leininger, and F. X. Gadea, *Phys. Rev. A* **63**, 062710 (2001).
- [35] J. Fedor, C. Winstead, V. McKoy, M. Čížek, K. Houfek, P. Kolorenc, and J. Horáček, *Phys. Rev. A* **81**, 042702 (2010).
- [36] M. Lowenthal, R. Khanna, and M. H. Moore, *Spectrochim. Acta A* **58**, 73 (2002).
- [37] I. I. Fabrikant, *J. Phys. B: Atom. Molec. Phys.* **49**, 222005 (2016).
- [38] Y. Itikawa, *Int. Rev. Phys. Chem.* **16**, 155 (1997).
- [39] M. Čížek, J. Horáček, M. Allan, and W. Domcke, *Czech. J. Phys.* **52**, 1057 (2002).
- [40] K. Houfek, *Nucl. Instr. Meth. Phys. Res. B* **279**, 71 (2012).
- [41] H. Hotop, M. Ruf, M. Allan, and I. I. Fabrikant, *Adv. At. Mol. Opt. Phys.* **49**, 85 (2003).
- [42] G. Gribakin, *Nucl. Instr. Meth. Phys. Res. B* **192**, 26 (2002).
- [43] M. Allan, M. Čížek, J. Horáček, and W. Domcke, *J. Phys. B* **33**, L209 (2000).
- [44] T. P. R. Kumar, J. Kočišek, K. Bravaya, and J. Fedor, *Phys. Chem. Chem. Phys.* **22**, 518 (2020).
- [45] M. Allan, *J. Phys. B: Atom. Molec. Phys.* **35**, L387 (2002).
- [46] G. Herzberg, *Molecular Spectra and Molecular Structure I: Spectra of Diatomic Molecules* (Van Nostrand, Princeton, New Jersey, 1950).
- [47] V. Laporta, J. Tennyson, and R. Celiberto, *Plasma Sources Sci. Technol.* **25**, 06LT02 (2016).